Elasticity of an Assembly of Disordered Nanoparticles Interacting *via* Either van der Waals-Bonded or Covalent-Bonded Coating Layers

Adil Ayouch,[†] Xavier Dieudonné,[‡] Gwenaëlle Vaudel,[†] Hervé Piombini,[‡] Karine Vallé,[‡] Vitalyi Gusev,[†] Philippe Belleville,[‡,*] and Pascal Ruello[†,*]

[†]Institut des Molécules et Matériaux du Mans, UMR CNRS 6283, Université du Maine, France and [‡]CEA, DAM, LE RIPAULT, F-37260 Monts, France

ABSTRACT Tailoring physical and chemical properties at the nanoscale by assembling nanoparticles currently paves the way for new functional materials. Obtaining the desired macroscopic properties is usually determined by a perfect control of the contact between nanoparticles. Therefore, the physics and chemistry of nanocontacts are one of the central issues for the design of the nanocomposites. Since the birth of atomic force microscopy, crucial advances have been achieved in the quantitative evaluation of van der Waals and Casimir forces in nanostructures and of adhesion between the nanoparticles. We present here an investigation, by a noncontact method, of the elasticity of an assembly of nanoparticles interacting *via* either van der Waals-bonded or covalent-bonded coating layers. We demonstrate indeed that the ultrafast opto-acoustic technique, based on the generation and detection of hypersound by femtosecond laser pulses, is very sensitive to probe the properties of the nanocontacts. In particular, we observe and evaluate how much the subnanometric molecules present at nanocontacts influence the coherent acoustic phonon propagation along the network of the interconnected silica nanoparticles. Finally, we show that this ultrafast opto-acoustic technique provides quantitative estimates of the rigidity/stiffness of the nanocontacts.

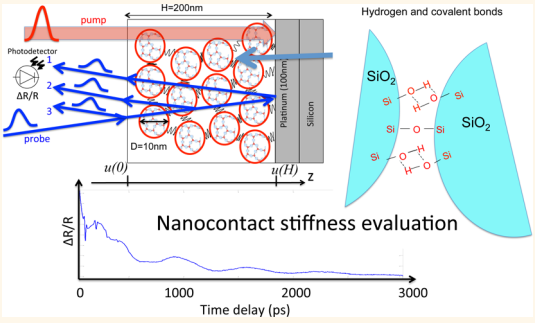

KEYWORDS: colloidal solids · physics and chemistry of nanocontacts · adhesion · time-resolved ultrafast opto-acoustics

Assembly of nanoparticles (colloidal films) is one of the most important techniques for the elaboration of a large variety of advanced thin film materials with targeted physical and chemical properties. Colloidal films are intrinsically nanocomposite systems made of surface interconnected nanoparticles (NPs) within a filling medium (air, liquid, polymer, *etc.*). By adjusting the nanoparticles' volume fraction, the intrinsic physical and chemical properties of nanoparticles, as well as the nature of the nanoparticles' interconnection, the physical and chemical properties of colloidal films can be designed for specific applications in optics,[1,2] plasmonics,[3] and photovoltaics.[4] Intense efforts have been made to control the growth of these nanoparticle assemblies.[5−8] Chemical routes to obtain colloidal films are numerous. Different types of chemical precursors as well as different solvents are employed to prepare thin films. Special care is often taken to prevent aggregation of nanoparticles in solution during the process which could lead to the desired nanostructure of the deposited colloidal film. Indeed, in order to manage the deposited film properties, nanoparticle-containing solutions need to be rheologically time-stable. To achieve this, several types of particle stabilizations are available: electrostatic, steric, or even haloing-type.[9,10] According to the adopted routes, the chemical nature of nanoparticles' surface is then often very different.[9] Moreover, surface chemical bonds affect the chemical stability of the system regarding some possible aggressive chemical environment (oxidation, hydration, *etc.*). These molecules involved in the NP interconnection also have a crucial role in the physical and chemical properties of the nanoparticle

* Address correspondence to pascal.ruello@univ-lemans.fr, philippe.belleville@cea.fr.

Received for review August 10, 2012 and accepted November 17, 2012.

Published online November 17, 2012
10.1021/nn303631d

assembly as mentioned above.[1−4] In particular, the chemical nature of the interconnecting molecules controls the mechanical cohesion, stability, and elasticity of the colloidal film. Knowing and controlling the strength of nanoparticle interconnections is indeed essential for the mechanical integrity of their assemblies. Moreover, elastic properties (sound speed and elastic modulus, for example) are basic physical parameters that must be known to understand heat conduction properties in such nanostructured systems. The colloidal film cohesion is not easy to evaluate since it is not easy in practice, first, to precisely control the nanoparticles' surface because of the sometimes rather complex chemical path to the final state. Second, even if the nanoparticle interconnecting molecules are perfectly known, it is not straightforward to relate quantitatively the elastic properties and cohesion of the entire material to their chemical nature. Only a few attempts have been done in disordered[11−14] or ordered assemblies of nanoparticles.[15,16] The nature of the chemical bonds cementing the nanoparticles in colloidal solids is typically established with light spectroscopy techniques such as IR spectroscopy and Raman spectroscopy.[17] These techniques provide reliable and precise information on the population of bonds involved in the particle interconnection which allows a prevision of some tendencies in the strength of the forces involved in the NPs' interconnection. However, these techniques do not characterize the cohesion/elasticity of the entire colloidal solid that is actually defined by the mechanical stability/rigidity of the nanoconnections between the particles. Near-field methods, such as atomic force microscopy, provide information on the elasticity but are limited to the near surface region of the material by definition.[18]

In this article, we evaluate the influence of the nature of the bonds of the chemical groups involved in the NPs' interconnection on the elastic properties of their disordered assembly by measuring the stiffness of the interparticle contacts. We show that changing only the chemical nature of the bonds in the molecules, which are connecting the particles, leads to dramatic variation of the velocity of sound propagation along the interconnected particle chains. In our experiments, the sound velocity in colloidal films was measured by all-optical contact-less monitoring of the mechanical resonances of the films with the use of the femtosecond laser. Our experimental investigations provide also an original way to estimate the surface energy of the NP covered by the molecules.

RESULTS

In order to demonstrate the strong influence on the colloidal film elastic properties of the chemical bonds in the chemical groups that interconnect NPs, experiments have been performed with canonical silica nanoparticles with variable surface energy. The colloidal films (CFs) are made of interconnected nanoparticles of well-defined diameter (10 nm) interacting either *via* van der Walls (VDW)-bonded ethoxy groups (−O−CH_2−CH_3) in samples 1 and 2 (denoted in the following as VDW-CF) or *via* hydrogen/covalent-bonded hydroxyl groups (OH−) in samples 3 and 4 (denoted as H-CV-CF; see Figure 1b). The studied colloidal samples are films of around 200 nm in thickness supported by the Si(100) substrate covered by a 100 nm thick layer of Pt. The colloidal films are obtained by dip-coating. A typical high-resolution electron microscope (HREM) image of nanoparticles in the solution is given in Figure 1a. The transformation of the VDW-bonded chemical groups into hydrogen/covalent bonded chemical groups is well-established[19−21] and is achieved according to two processes (process 1 and 2) detailed in Methods as well as in the Supporting Information. The refractive index of H-CV-CF and VDW-CF and their thicknesses were measured by multiple wavelength ellipsometry,[22] and the values are given in Table 1. The refractive index and thus the film porosity remain nearly the same whatever the nature of the chemical groups coated onto nanoparticles. This shows that the colloidal thin film undergoes no damage during wiping operations. Moreover, that absence of a modification of the refractive index is also consistent with the expectations that the volume occupied by the surface bonds of NPs is negligible compared to the total volume. The lengths of the surface molecules are indeed very small compared to the diameters of silica spheres with around 0.5 nm for the ethoxy molecules C_2H_5O and around 0.1 nm for the OH group.[23] Consequently, the transition from VDW to H-C coating chemical groups affects neither the volume concentration of bounded electrons that drives the dielectric response in the visible range nor the mass density of the film. Two reference dense films have also been prepared. A film of polymeric silica has been obtained by sol−gel method (sample 5) and dense silica film (denoted as PVD, sample 6) by physical vapor deposition. Their characteristics are given in Table 1.

The elasticity of the 3D assembly of interconnected particles was evaluated by applying the all-optical ultrafast acoustics method (see Methods). This method consists in the generation and detection by a femtosecond laser of coherent acoustic waves of GHz−THz frequencies. This noncontact technique is an all-optical technique that is a powerful tool to evaluate elastic properties of thin films,[24] as well as to reveal nanoscale elastic and optical inhomogeneities.[25,26] The pump femtosecond laser pulse generates first a short acoustic pulse in the opaque platinum film (see Figure 2a). A part of the acoustic field is then transmitted into the colloidal film and induces mechanical vibrations of the colloidal film. These vibrations modify the optical reflectivity R of the system through various physical mechanisms.[24] Acoustically induced changes in optical reflectivity can be detected with the femtosecond

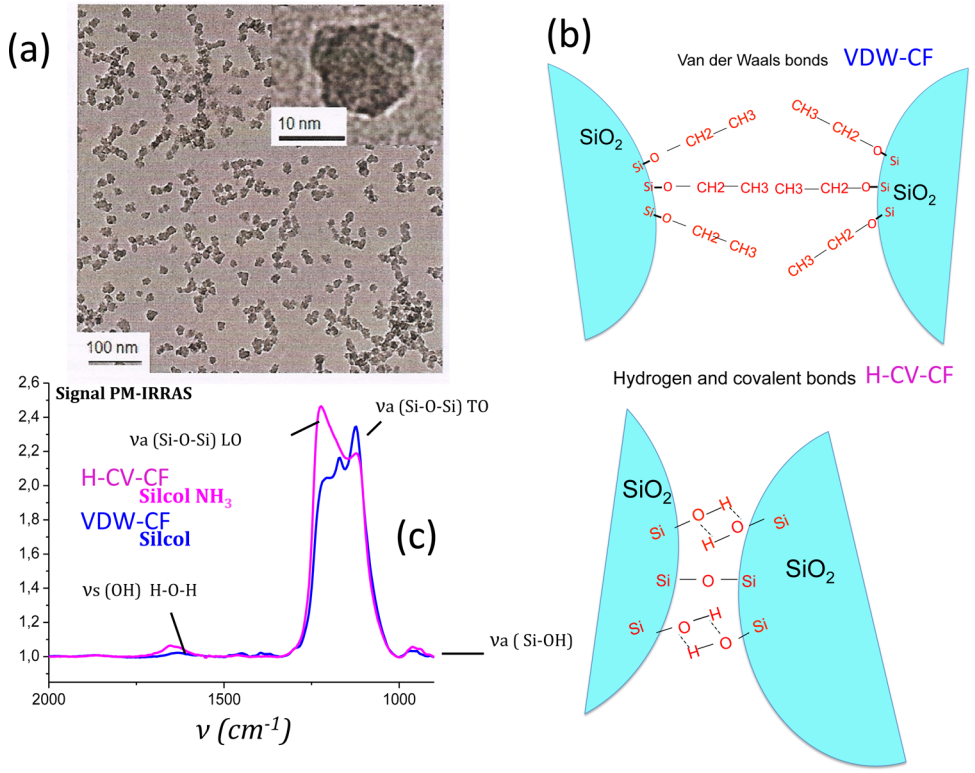

Figure 1. (a) High-resolution electron microscopy (HREM) image of the nanoparticles in solution before the colloidal film preparation by dip-coating. (b) Sketch of the van der Waals and covalent hydrogen interactions between nanoparticles in the dip-coated colloidal films. (c) PM-IRRAS spectra (2000−900 cm^{-1}) of colloidal silica films with (SILCOL NH3) and without NH_3 curing (SILCOL). The increase of the Si−O−Si LO asymmetric stretching vibration band at 1220 cm^{-1} and of the 1650 cm^{-1} OH vibration band is interpreted to result from a strengthening of silicate gel network through cross-linking for hydrogen/covalent-bonded colloidal film (H-CV-CF).

TABLE 1. Characteristics of the Disordered Assemblies of Nanoparticles (Colloidal Film) and of the Reference Films: Measured Optical Properties, Acoustic Properties, and Elastic Properties, and Deduced Nanocontact Stiffness and Nanoparticle Surface Energy

	optical characterizations			acoustic eigenmodes frequencies		sound velocity	elastic modulus	effective NPs contact stiffness (J/m^2)	NP surface energy (J/m^2)
samples	H (nm) ± 2 nm	opt. index n ± 0.01	porosity P	f_0 (GHz)	f_1 (GHz)	V (m/s) (err. 5%)	M (GPa)	k_{eff}	$\gamma/2$
colloidal films									
sample 1: SiO_2 NPs (VDW) native film	191	1.21	55	1.5	4.6	1160	1. 3	35	0.002
sample 2: SiO_2 NPs (VDW) native film	210	1.21	55	1.7	5.1	1430	1.9	58	0.009
sample 3: SiO_2 NPs (H-CV) process 1	194	1.22	54	2.6	7.7	1990	3.9	103	0.050
sample 4: SiO_2 NPs (H-CV) process 2	210	1.21	55	2.2	6.4	1800	3.1	85	0.028
reference films									
sample 5: SiO_2 polymeric	176	1.4	12.7	5.4	17	3970	27.8		
sample 6: SiO_2 PVD	200	1.45		6.7	20.1	5360	64		
sample 7: platinum (Pt/Si)	100								

probe laser pulses, as depicted in Figure 2a. In Figure 3a, the measured transient optical reflectivity $\Delta R(t)$ is presented for the different samples of 3D interconnected NPs. The transient optical reflectivity signals recorded over a time scale of more than 1.5 ns exhibit periodic oscillations whose period drastically depends on the film preparation process that is on the nature of the interparticle nanocontacts (Figure 3a). An experiment was also conducted with a platinum film deposited onto the silicon without colloidal films (sample 7). The signal reveals periodic pulsed changes in transient reflectivity taking place every 100 ps. This is a well-known[24] manifestation of the acoustic echoes in the thin film following its excitation by femtosecond laser. In this case, the photogenerated acoustic pulses in Pt travel back and forth and are partially reflected at

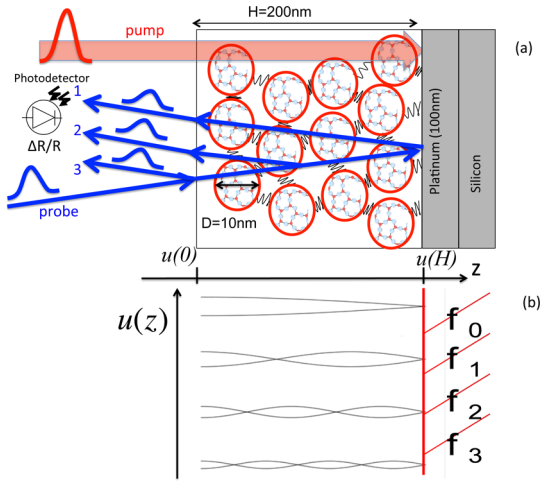

Figure 2. (a) Principle of the ultrafast acoustic pump−probe experiment performed on the nanoparticles thin film deposited onto the Pt/Si substrate. (b) Representation of the first four eigenmodes of the colloidal film mechanical resonance with $f_n = (2n + 1)V_{LA}/4H$, where n, V_{LA}, and H are the index of the mode, the longitudinal sound velocity in the colloidal film, and the colloidal film thickness, respectively.

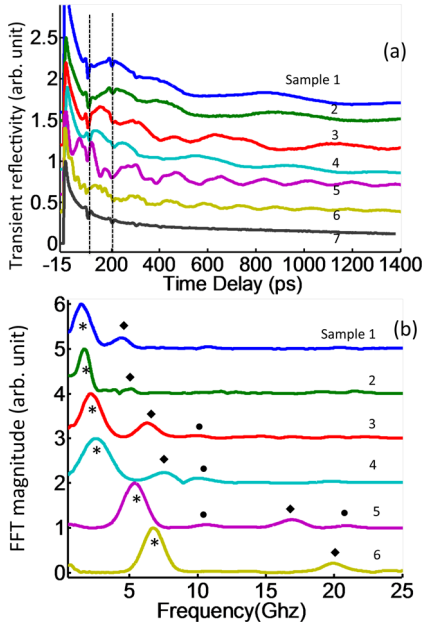

Figure 3. (a) Transient reflectivity measurements performed on each system whose properties are described in Table 1. The long-living oscillatory parts of the optical reflectivity, which are clearly visible, are due to the mechanical resonances (see Figure 2b) induced by the laser pump excitation. (b) Fast Fourier transform of the transient reflectivity signals. The star and the diamond indicate the two first eigenmodes with frequency f_0 and f_1 (see Figure 2b). The circle indicates acoustic components coming from the photoinduced acoustic modes in the platinum layer embedded between the silicon substrate and the nanoparticle assembly thin film.

the Pt/Si interface. Each acoustic echo occurring around every 100 ps is optically detected on the mechanically free surface of Pt film, where they exhibit 100% reflection. These echoes are observed in all signals obtained with NP films (Figure 3a). However, they are not important to our method of colloidal film evaluation. We are interested only in the components of the signals having the form of continuous sinusoidal oscillations. The Fourier transforms of the time-resolved transient optical reflectivity signals are given in Figure 3b. Additionally, to the main vibratory component at frequency f_0 that is also easily distinguishable in the time domain (Figure 3a), a second mode is present with a frequency f_1, which is approximately three times higher than f_0 (see FFT). The existence of a ratio very close to 3 between the frequencies of the two detected vibration modes in all of the films indicates that these two modes are standing acoustic waves of the colloidal film (see the eigemodes structure in Figure 2b). These frequencies verify the following sequence of eigenmodes frequencies f_n of a film with one surface bounded onto a rigid substrate and another surface being mechanically free:

$$f_n = (2n+1)\frac{V_{LA}}{4H} \quad (1)$$

where $n = 0, 1, 2, 3...$, V_{LA} is the longitudinal sound speed, and H is the film thickness. Equation 1 describes the so-called quarter-wavelength resonances. The first and second eigenmodes correspond to $n = 0$ (f_0) and $n = 1$ (f_1), respectively. These acoustic eigenmodes correspond to a collective displacement of the assembly of interconnected NPs depicted in Figure 2b. The maximum of the particle displacements takes place at the free surface of the colloidal film. The displacement of the CF/Pt interface is much smaller because of the huge difference in the acoustic impedances of the soft colloidal film and platinum. The possibility of excitation and detection of such "closed-pipe organ-like" acoustic eigenmodes has been recently reported in different submicrometric films either by ultrafast opto-acoustics technique[27,28] or by Brillouin light scattering[29] but has never been applied before for the diagnostics of the disordered assemblies of nanoparticles.

The determination of these eigenmode frequencies allows direct determination of the sound speed V_{LA} by a linear mean least-squares fit of two first eigenmode frequencies (Table 1). The determined velocities of the longitudinal acoustic wave can be used for the evaluation of the so-called longitudinal (or "pressure wave") modulus M, using the relation $M = \rho V_{LA}^2$, provided that the information on the films densities is available. To estimate the densities, we first used the knowledge of the optical refractive indexes to estimate the porosities of the films with the help of the Maxwell−Garnett relations.[30] For a refractive index of 1.22, we estimate a porosity p of 55%. This consequently leads to the solid state fraction φ of 45% in the film and an effective density of the film $\rho = 990$ kg/m^3, assuming the density of silica to be 2200 kg/m^3. The effective elastic longitudinal moduli M can then be determined (Table 1).

It should be first mentioned that the estimated value of the modulus found for dense PVD silica film (sample 6) is in agreement with literature.[31] The polymeric film (sample 5) exhibits smaller elastic modulus essentially due to its nonzero porosity. All assemblies of NPs exhibit elastic moduli that are smaller than 5 GPa, that is, more than 5 times lower than in polymeric film, more than an order of magnitude smaller than in dense silica film, and more that 20 times lower than the longitudinal modulus of bulk fused silica, which is 78.5 GPa. The blue shift of eigenmode frequencies in a transition from a VDW-CF to a H-CV-CF (see Table 1) is a clear manifestation of the 2−3-fold increase of the elastic modulus M in colloidal films, where the contacts between the nanoparticles are supported by the chemical groups/layers with hydrogen/covalent bonds, in comparison with the films, where these contacts are supported by the chemical groups/layers with VDW bonds.

DISCUSSION

The existing theories for the elasticity of granular assemblies[32−34] provide the opportunity to get a better understanding of the physics of the elastic response of the colloidal films and additional information on their micromechanical parameters. In particular, the rigidity/stiffness of the individual contacts between the assembled nanoparticles can be estimated. Indeed, the theories[32−34] predict the dependencies of the effective Lame constants λ and μ of the granular assemblies on the normal k_n and transversal k_t rigidities/stiffnesses of the individual contacts:

$$\lambda = \frac{z\varphi}{5\pi d}(k_n - k_s), \quad \mu = \frac{z\varphi}{10\pi d}(2k_n - 3k_s) \qquad (2)$$

Here, z is the average number of contacts per particle, called coordination number, φ is the solid volume fraction, already defined earlier, and d is the diameter of the spherical particles.

With the help of eq 2, using the known relation between the longitudinal and Lame moduli, that is, $M = \lambda + 2\mu$, and the relation $\rho = \varphi m/(\pi d^3/6)$ of the film density to the masses m of the individual nanoparticles, the expression for the speed of the longitudinal acoustic wave in the nanogranular film can be presented in the form

$$V_{LA} = \sqrt{\frac{M}{\rho}} = d\sqrt{\left(\frac{z}{10}\right)\left(\frac{k_n + (2/3)k_s}{m}\right)} \qquad (3)$$

Equation 3 demonstrates that the sound velocity actually does not depend directly/explicitly on the solid volume fraction or film density. The important parameters controlling the speed of sound propagation are the coordination number and the stiffnesses of the individual contacts. Additional insight is provided by comparison of eq 3 with the classical solution for the longitudinal acoustic velocity in one-dimensional straight chain of particles[35] $V_{LA} = d(k_n/m)^{1/2}$. Similar to the 1D case, the sound velocity in 3D assembly of nanoparticles is controlled by the characteristic frequency of the local vibrations of the lumped masses on the springs; however, in the 3D assembly, the shear rigidity of the contacts contributes importantly to effective stiffness of the contacts $k_{eff} = k_n + (2/3)k_s$, which influences the longitudinal sound propagation. In order to determine with the help of eq 3 the effective stiffness of the contacts in the studied colloidal films from the measured sound velocities, the information on the coordination number z is necessary. It is well-known that in noncohesive granular assemblies the estimation of the coordination number is difficult because of the absence of the one-to-one relation between the sample porosity and the coordination number of particles.[36] By different assembling procedures, it is possible to prepare at fixed external pressure the samples of the same density but with different coordination numbers and *vice versa*. The situation with cohesive assemblies of spherical particles is more definite. Rather different simulations[37,38] predict quantitatively the expected tendency of the fall in the coordination number of particles z either with the diminishing solid volume fraction φ or with growing porosity p. The relations $z = 1.126\exp(3.196\varphi)$ from ref 37 and $z = 3.08/p - 1.13$ from ref 38 predict for our samples of 55% porosity the coordination numbers 4.7 and 4.5, respectively. In Table 1, we present the estimates of the effective rigidities k_{eff} of the nanocontacts obtained with $z = 4.6$.

For the sake of comparison, it would be instructive to estimate the rigidities of the contacts that could be achieved in the assembly of the naked/bare silica nanoparticles due to adhesion caused by their interaction *via* VDW forces.[39] Using the theoretical value[39] of the Hamaker constant $A = 6.5\ 10^{-20}$ J and assuming the equilibrium intermolecular distance to be $b \approx 0.28$ nm, an average between atomic separation of O−O pairs at 0.26 nm and of Si−Si pairs at 0.31−0.32 nm evidenced by X-ray experiments,[40] we first estimate the interfacial energy of fused silica[39] $\gamma = A/(12\pi b^2) \approx 0.022$ J/m^2, which is on the order of the values experimentally measured in the setup based on the principles of AFM[41] ($\gamma_{exp} \approx 0.028$ J/m^2). The knowledge of the interfacial energy, of the Young modulus, $E = 73$ GPa, and the Poisson's ratio, $\nu = 0.17$, of the fused silica provides opportunity to estimate the so-called Maugis parameter[42,43] for the interaction between the two spheres of equal diameters $1.157[(1 - \nu^2)\gamma/E]^{2/3}d^{1/3}/b \approx 0.04$. The fact that the parameter is smaller than 0.1 indicates that VDW interaction forces between silica spheres of 10 nm diameter are long-range in comparison to elastic deformation of the nanoparticles they cause. In this case, the contact area is described by the Derjaguin−Muller−Toporov (DMT) regime,[44] which applies to rigid systems, low adhesion, and small

radii of curvature of the contacting surfaces and takes into account long-range attraction around the periphery of the contact area.[45] The interaction of a spherical particle of radius R with the plane surface is described in the DMT regime by[45] $P = Ka^3/R - 2\pi R\gamma$, $\delta = a^2/R$, where for a similar material of the particle and of the surface, the combined elastic modulus K is $K \equiv (2/3)E/(1 - \nu^2) \cong 50$ GPa for fused silica, δ is the mutual approach or relative displacement of the particle and the surface and P is the applied force. For the interaction between two spheres of the same diameter d, we substitute the effective radius $R = d/4$ and arrive to the following estimates of the contact parameters in the absence of the externally applied load, that is, when $P = 0$: the contact radius is $a = [\pi d^2\gamma/(8K)]^{1/3} \approx 0.25$ nm, the mutual approach of the nanoparticles is $\delta = 2a^2/d \approx 0.012$ nm and the normal stiffness of the contact is $k_n \equiv \partial P/\partial\delta = 3Ka \approx 37.5$ J/m^2. Assuming that the relation between the transversal and normal contact stiffnesses, which is valid for Hertzian contacts,[46] $k_t = [(2 - 2\nu)/(2 - \nu)]k_n$, approximately holds in the DMT regime, we arrive to the final estimate of the effective stiffness of the contact between silica nanoparticles: $k_{eff} = k_n + (2/3)k_s \approx 60.5$ J/m^2 ≈ 378 eV/(nm)^2. The comparison of these estimates with the effective stiffness coefficient k_{eff} presented in Table 1 demonstrates that the stiffness of the contacts in our VDW-CF samples is nonmodified or a bit diminished relative to the contact stiffness in the hypothetical assembly of naked/bare silica nanoparticles. This could be expected because of the VDW character of the molecular bonds in the coating chemical groups in our VDW-CF samples 1 and 2. In contrast, the contacts between the nanoparticles in the H-CV-CF samples 3 and 4, supported by the chemical groups with hydrogen/covalent bonds, are 30−70% stiffer than in pure silica assembly.

It is worth noting that both in the DMT regime, presented above, and in the Johnson−Kendall−Roberts (JKR) regime,[11,47] which applies to compliant materials, strong adhesion forces, and large radii of curvature of the contacting surfaces, the contact stiffness scales as a cubic root of interfacial energy $k_n \propto \gamma^{1/3}$. Because of this, even a marginal increase in the stiffness of the contacts requires important increase in effective interfacial energies. Our experimental data for surface energies $\gamma/2$, which are twice smaller than interfacial energies γ (Table 1) demonstrate that the effective surface energy of the nanoparticles in the H-CV-CF samples had been increased by the preparation process from 2 up to 4 times relative to the experimental value of the surface energy of fused silica $\gamma_{SiO_2} \approx 0.014$ J/m^2.[41] The interfacial energies of thus coated nanoparticles vary from 0.028 up to 0.050 J/m^2.

Our experimental results are in very good accordance with the expectations based on the theoretical predictions. Indeed, the theory of forces between two surfaces with coating layers[39,48] states that at separations less than the thickness of the coating layers the van der Waals interaction is dominated by the properties of the coating layers. "In particular, this means that the adhesion energies are largely determined by the properties of any adsorbed films even when these are only a monolayer thick" (ref 39, page 207). Our experimental observations are in accordance with the fact that the experimental value of the surface energy/tension of the ethanol $\gamma_{C_2H_5OH} \approx 0.020$ J/m^2 is importantly, that is, nearly 4 times lower than the experimental value of the surface energy/tension of hydrogen peroxide $\gamma_{H_2O_2} \approx 0.076$ J/m^2.[39] At the same time, our measurements clearly indicate that the procedures necessary for the assemblage of the colloidal films diminished the surface energies of the coated nanoparticles relative to these theoretical values. Our experimental results on VDW-CF (samples 1 and 2) indicate that the surface energy of nanoparticles with coated ethoxy groups is at least twice smaller than the surface tension of ethanol and even lower than the experimental values of the surface energy of bare silica nanoparticles. The results on H-CV-CF (samples 3 and 4) indicate that the surface energy of nanoparticles with coated OH groups is also about two times (1.4−2.4 times) smaller than the surface energy of hydrogen peroxide, but it is 2−4 times higher than the surface energy of bare silicon nanoparticles, as it has been already mentioned earlier.

Thus, we believe that the important result of our experimental measurements is that by using the molecular layers with high surface energy/tension for coating of the nanoparticles, it is possible to increase the rigidities of the interparticle contacts and of the colloidal films. In particular, with the use of OH groups, which are an essential part of such highly polar H-bonded liquids as H_2O_2 and H_2O, for example, it is possible to assemble the colloidal films with the elastic moduli up to 3 times higher than that in the films obtained with the use of ethoxy groups, originating from C_2H_5OH, whose surface energy is well-described by van der Waals interactions.

CONCLUSION

In conclusion, we have demonstrated that the investigation of elasticity of the assembly of NPs by acoustic nanowaves reveals the information on the stiffness of the interparticle contacts and on NPs' surface energy through an indirect way. We did not measure directly the interaction forces, but we extract the information on the interactions between the nanoparticles by measuring the propagation velocity of the acoustic waves. This is a contact-less method which is not restricted to surface analysis. Thanks to a very well-controlled and characterized nanoparticle surface chemistry, we demonstrated that the transition from van der Waals to hydrogen/covalent bonds of the NP coating layer induces strong variation of the elastic properties, and quantitative estimates are provided due to high sensitivity of acoustic phonon transport

through subnanometric interparticle contacts to contact stiffness. In association with surface chemistry control, the application of an opto-acoustic technique appears to be a very convenient tool for control of desired modifications of the macroscopic physical properties of functional nanomaterial-based coatings.

METHODS

Chemical Control of the Nanoparticles Interconnections. The transformation of the VDW-bonded chemical groups into hydrogen/covalent-bonded chemical groups is achieved thanks to the surface chemical condensation. The transformation takes place either by NH_3 vapor curing of the film during several hours (process 1 for sample 3)[19,20] or during the preparation of the colloid using an aging process in pH 9 alkaline solution conditions that promote interparticle bonding through vicinal species condensation reaction (process 2 for sample 4). Sample 1 (sample 2) is obtained from the same batch as sample 3 (sample 4) but has not been treated by the process 1 (process 2). Therefore, samples 1 and 2 are VDW-bonded colloidal films, named in Table 1 as native colloidal films. These chemical preparations allow advanced control of the interparticle bonding strength using easy and reproducible processes. High-resolution surface IR spectroscopy (PMIRRAS) has been performed to clearly demonstrate the chemical modification of the nanoparticle surfaces. Figure 1c shows comparison between infrared absorption response of standard and NH_3 post-treated silica layers, revealing obvious chemical changes due to the ammonia treatment. All IR bands can be assigned either to Si−O, Si−OH, or OH bond vibrations or to remaining ethoxy groups (bands appearing in the 1400 cm^{-1} region). After treatment, a strong modification occurred in the relative intensity of the Si−O−Si stretching broad band. The increase of the Si−O−Si LO asymmetric stretching vibration band at 1220 cm^{-1} and of the 1650 cm^{-1} OH vibration band is interpreted to result from a strengthening of silicate gel network through cross-linking which is, in general, strongly correlated to increasing physical properties such as microhardness.[12] As already mentioned, the ammonia treatment effect on colloidal silica layers is consistent with the base-catalyzed condensation mechanism proposed by Iler.[21] With ammonia curing, the particle-to-particle linking is enhanced *via* H-bonding of neighbor particles through vicinal silanols and condensation reactions *via* siloxane bridging.

Ultrafast Acoustic Methods. The photogeneration and photodetection of mechanical resonance of colloidal films (see vibration eigenmodes as depicted in Figure 2b) are achieved thanks to a pump−probe experiment. A Ti:sapphire Kerr mode-locked pulsed femtosecond laser is employed where the laser beam is separated into a pump pulse (excitation) and a probe pulse (detection). In our experiments, the pump and probe wavelengths were 800 and 400 nm, respectively. At these wavelengths, the light absorption by the silica colloidal film is negligible. The pump photoinduced mechanical vibrations of the colloidal film modulate the optical reflectivity R of the probe beam. These variations of the probe optical reflectivity R, denoted as $\Delta R/R$, are collected by a balanced photodiode and processed with a lock-in amplifier. The time-resolved measurement is accomplished by a probe pulse delayed in time relative to the pump pulse with a moving mirror that permits control of the probe beam optical path (*i.e.*, the arrival time of the probe pulse on the sample).

Conflict of Interest: The authors declare no competing financial interest.

Acknowledgment. A.A., G.V., V.G., and P.R. acknowledge funding from CPER Pays de la Loire program. X.D., H.P., K.V., and P.B. acknowledge C. Méthivier and C.-M. Pradier from the Surface Reactivity Laboratory in University of Paris (Paris VI) for FT IRRAS measurements.

Supporting Information Available: All-optical ultrafast acoustic method based on the pump and probe scheme, the polarization modulated infrared reflection absorption spectroscopy (PM-IRRAS) and the sample preparation description are fully described in the Supporting Information. This material is available free of charge *via* the Internet at http://pubs.acs.org.

REFERENCES AND NOTES

1. Daniel, M.-C.; Astruc, D. Gold Nanoparticles: Assembly, Supramolecular Chemistry, Quantum-Size Related Properties, and Applications towards Biology, Catalysis and Nanotechnology. *Chem. Rev.* **2004**, *104*, 293–346.
2. Belleville, P.; Bonnin, C.; Priotton, J.-J. Room-Temperature Mirror Preparation Using Sol−Gel Chemistry and Laminar-Flow Coating Technique. *J. Sol−Gel Sci. Technol.* **2000**, *19*, 223–226.
3. Oonishi, T.; Sato, S.; Yao, H.; Kimura, K. Three-Dimensional Gold Nanoparticle Superlattices: Structures and Optical Absorption Characteristics. *J. Appl. Phys.* **2007**, *101*, 114314.
4. Saunders, B.; Turner, M. Nanoparticle-Polymer Photovoltaic Cells. *Adv. Colloid Interface Sci.* **2008**, *138*, 1–23.
5. Min, Y.; Akbulut, M.; Kristiansen, K.; Golan, Y.; Israelachvili, J. Role of Interparticle and External Forces on the Assembly and Properties of Nanoparticle Materials. *Nat. Mater.* **2008**, *7*, 527–538.
6. Oaki, Y.; Anzai, T.; Imai, H. Homogeneous and Disordered Assembly of Densely Packed Nanocrystals. *Adv. Funct. Mater.* **2010**, *20*, 4127–4132.
7. Klajn, R.; Bishop, K. J.; Grzybowski, B. A. Light-Controlled Self-Assembly of Reversible and Irreversible Nanoparticle Suprastructures. *Proc. Natl. Acad. Sci. U.S.A.* **2007**, *104*, 10305–10309.
8. Park, J.; Zheng, H.; Lee, W. C.; Geissler, P. L.; Rabani, E.; Alivisatos, A. P. Direct Observation of Nanoparticle Superlattice Formation by Using Liquid Cell Transmission Electron Microscopy. *ACS Nano* **2012**, *6*, 2078–2085.
9. Jolivet, J. P.; Henry, M.; Livage, J. *Metal Oxide Chemistry and Synthesis*; John Wiley and Sons: New York, 1994.
10. Tohver, V.; Samy, J. E.; Braem, A.; Braun, P. V.; Lewis, J. A. Nanoparticle Halos: A New Colloid Stabilization Mechanism. *Proc. Natl. Acad. Sci. U.S.A.* **2001**, *98*, 8950–8954.
11. Kendall, K.; Alford, N. M.; Birchall, J. D. A New Method for Measuring the Surface Energy of Solids. *Nature* **1987**, *325*, 794–796.
12. Muller, V. M.; Derjaguin, B. V.; Toporov, Y. P. On Two Methods of Calculation of the Force of Sticking of an Elastic Sphere to a Rigid Plane. *Colloids Surf.* **1983**, *7*, 251–259.
13. Zahn, K.; Wille, A.; Maret, G.; Sengupta, S.; Nielaba, P. Elastic Properties of 2D Colloidal Crystals from Video Microscopy. *Phys. Rev. Lett.* **2003**, *90*, 155506.
14. Ogawa, K.; Vogt, T.; Ullmann, M.; Johnson, S.; Friedlander, S. K. Elastic Properties of Nanoparticle Chain Aggregates of TiO_2, Al_2O_3, and Fe_2O_3 Generated by Laser Ablation. *J. Appl. Phys.* **2000**, *87*, 63.
15. Mattarelli, M.; Montagna, M.; Still, T.; Schneider, D.; Fytas, G. Vibration Spectroscopy of Weakly Interacting Mesoscopic Colloids. *Soft Matter* **2012**, *8*, 4235.
16. Lisiecki, I.; Halté, V.; Petit, C.; Pileni, M.-P.; Bigot, J.-Y. Vibration Dynamics of Supra-Crystals of Cobalt Nanocrystals Studied with Femtosecond Laser Pulses. *Adv. Mater.* **2008**, *20*, 4176–4179.
17. Chassaing, P.-M.; Demangeot, F.; Combe, N.; Saint-Macary, L.; Kahn, M. L.; Chaudret, B. Raman Scattering by Acoustic Phonons in Wurtzite ZnO Prismatic Nanoparticles. *Phys. Rev. B* **2009**, *79*, 155314.
18. Bhushan, B. *Scanning Probe Microscopy in Nanoscience and Nanotechnology*; Springer: Berlin, 2010.
19. Belleville, P.; Floch, H.; Pegon, M. Sol−Gel Broadband Antireflective Coatings for Advanced Laser-Glass Amplifiers. *SPIE Proc. 2288, Sol−Gel Optics III*, San Diego, CA, 1994; p 25

20. Belleville, P.; Floch, H. French Patent 9303987 assigned to CEA.
21. Iler, R. K. *The Chemistry of Silica*; Wiley: New York, 1979.
22. Azzam, R. M. A.; Bashara, N. M. *Ellipsometry and Polarized Light*, 1st ed.; North-Holland Publishing Company: Amsterdam, 1977.
23. Dean, J. A. *Lange's Handbook of Chemistry*, 15th ed.; McGraw Hill Book Co.: New York, 1999.
24. Thomsen, C.; Grahn, H. T.; Maris, H. J.; Tauc, J. Surface Generation and Detection of Phonons by Picosecond Light Pulses. *Phys. Rev. B* **1986**, *34*, 4129–4132.
25. Mechri, C.; Ruello, P.; Breteau, J. M.; Baklanov, M. R.; Verdonck, P.; Gusev, V. Depth-Profiling of Elastic Inhomogeneities in Transparent Nanoporous Low-k Materials by Picosecond Ultrasonic Interferometry. *Appl. Phys. Lett.* **2009**, *95*, 091907.
26. Lomonosov, A. M.; Ayouch, A.; Ruello, P.; Vaudel, G.; Baklanov, M. R.; Verdonck, P.; Zhao, L.; Gusev, V. E. Nanoscale Noncontact Subsurface Investigations of Mechanical and Optical Properties of Nanoporous Low-k Material Thin Film. *ACS Nano* **2012**, *6*, 1410–1415.
27. Mechri, C.; Ruello, P.; Gusev, V. Confined Coherent Acoustic Modes in a Tubular Nanoporous Alumina Film Probed by Picosecond Acoustics Methods. *New J. Phys.* **2012**, *14*, 023048.
28. Akimov, A. V.; Young, E. S. K.; Sharp, J. S.; Gusev, V.; Kent, A. J. Coherent Hypersonic Closed-Pipe Organ Like Modes in Supported Polymer Films. *Appl. Phys. Lett.* **2011**, *99*, 021912.
29. Zhang, X.; Sooryakumar, R.; Every, A. G.; Manghnani, M. H. Observation of Organ-Pipe Acoustic Excitations in Supported Thin Films. *Phys. Rev. B* **2001**, *64*, 081402.
30. Choy T. C. *Effective Medium Theory*; Oxford: New York, 1999.
31. *Handbook of Chemistry and Physics*, 76th ed.; CRC Press: Roca Raton, FL, 1995−1996.
32. Digby, P. The Effective Elastic Moduli of Porous Granular Rock. *J. Appl. Mech.* **1981**, *48*, 803–808.
33. Walton, K. The Effective Elastic Moduli of a Random Packing of Spheres. *J. Mech. Phys. Solids* **1987**, *35*, 213–226.
34. Suiker, A. S. J.; de Borst, R.; Chang, C. S. Micromechanical Modeling of Granular Material. Part 1: Derivation of a Second-Gradient Micro-Polar Constitutive Theory. *Acta Mech.* **2001**, *149*, 161–180.
35. Kittel, C. *Introduction to Solid State Physics*; Wiley: New York, 1996.
36. Agnolin, I.; Roux, J.-N. Internal States of Model Isotropic Granular Packings. I. Assembling Process, Geometry, and Contact Networks. *Phys. Rev. E* **2007**, *76*, 061302.
37. Norman, L. D.; Maust, E. E. Computer Simulation of Particulate System. *Nev. Bur. Mines, Bull.* **1971**, *658*, 35–48.
38. van de Lagemaat, J.; Benkstein, K. D.; Frank, A. J. Relation between Particle Coordination Number and Porosity in Nanoparticle Films: Implications to Dye-Sensitized Solar Cells. *J. Phys. Chem. B* **2001**, *105*, 12433–12436.
39. Israelashvili, J. N. *Intermolecular and Surface Forces*; Academic Press: London, 1992.
40. Henningen, E. H.; Buschert, R. C.; Heaton, L. Atomic Structure and Correlation in Vitreous Silica by X-ray and Neutron diffraction. *J. Phys. Chem. Solids* **1967**, *28*, 423–432.
41. Heim, L.-O.; Blum, J.; Preuss, M.; Butt, H.-J. Adhesion and Friction Forces between Spherical Micrometer-Sized Particles. *Phys. Rev. Lett.* **1999**, *83*, 3328–3331.
42. Carpick, R. W.; Oglette, D. F.; Salmeron, M. A. General Equation for Fitting Contact Area and Friction *vs* Load Measurements. *J. Colloid Interface Sci.* **1999**, *211*, 395400.
43. Maugis, D. J. Adhesion of Spheres: The JKR-DMT Transition Using a Dugdale Model. *Colloids Interface Sci.* **1992**, *150*, 243–269.
44. Derjaguin, B. V.; Muller, V. M.; Toporov, Y. P. Effect of Contact Deformations on the Adhesion of Particles. *J. Colloid Interface Sci.* **1975**, *53*, 314–326.
45. Burnham N. A.; Kulik, A. J. Surface Forces and Adhesion. In *Handbook of Micro/Nano Tribology*; Brushan, B., Ed.; CRC Press: Boca Raton, FL, 1999; pp 247−271.
46. Johnson, K. L. *Contact Mechanics*; Cambridge University Press: Cambridge, 1985.
47. Johnson, K. L.; Kendall, K.; Roberts, A. D. Surface Energy and the Contact of Elastic Solids. *Proc. R. Soc. London A* **1971**, *324*, 301.
48. Israelachvili, J. N. The Calculation of van der Waals Dispersion Forces between Macroscopic Bodies. *Proc. R. Soc. A* **1972**, *331*, 39–55.